RECENT PROGRESSES ON THE RMP RESEARCHES TOWARDS ACTIVE CONTROL OF TEARING MODE IN THE J-TEXT TOKAMAK

D Li[1], Y H Ding[1]*, N C Wang[1], B Rao[1], Q M Hu[2], H Jin[5], M Li[1], Z Huang[1], Z Song[1], S Zhou[1], J Li[6], M Yan[1], G Xu[1], X Ji[1], R Jia[1], L Peng[1], Y He[1], Q Zhang[1], W Zhang[1], J Dong[1], Q. Yu[3], Y. Liang[1,4] and the J-TEXT team

[1]International Joint Research Laboratory of Magnetic Confinement Fusion and Plasma Physics, State Key Laboratory of Advanced Electromagnetic Engineering and Technology, School of Electrical and Electronic Engineering, HUST, China

[2]Princeton Plasma Physics laboratory, US

[3]Max-Planck-Institut für Plasmaphysik, 85748 Garching, Germany

[4]Forschungszentrum Jülich GmbH, 52425 Jülich, Germany

[5]College of Electrical and Information Engineering, Lanzhou University of Technology, Lanzhou, China.

[6]Advanced Energy Research Center, Shenzhen University, Shenzhen, China

*Corresponding Author: Y H Ding, yhding@hust.edu.cn

Abstract:

Controlling the tearing mode (TM) is one of the major topics of fusion research, since TM degrades the plasma confinement and even induces major disruption if it is locked. Previous experimental and theoretical studies showed that the resonant magnetic perturbations (RMPs) influence both the rotation and width of the TM. Based on these effects, two strategies for controlling the TM have been proposed and tested on J-TEXT by applying the pulsed or fast rotating RMPs. The first control strategy is to apply pulsed RMP to the TM only during the accelerating phase region. By nonlinear numerical modelling, it is proved efficient in accelerating the mode rotation and even completely suppresses the mode. The followed experimental attempt with the pulsed RMP at relative low amplitude has demonstrated the acceleration effect. Secondly, the fast rotating RMP field has been successfully applied before the mode locking and avoided the mode locking and the following disruption. The experiment results of applying rotating RMPs with different frequency and amplitude were carried out and suggested that the rotating RMP with higher frequency is more advantageous to the disruption control. As a result, the disruption was prevented.This paper will present these recent efforts.

1. INTRODUCTION :

Tearing mode (TM) [1, 2], especially the m/n = 2/1 TM, deteriorate the confinement performance significantly, where m and n are the poloidal and toroidal mode numbers respectively. In addition, the TM could be decelerated to a non-rotating state, leading to the so called locked mode (LM)[3]. The LM usually grows to a very large amplitude, and it is one of the most common causes of major disruption [4] in a tokamak. Therefore, active control of the TM is an important issue for future fusion reactors, e.g. ITER [5,6] and CFETR [7]. In this paper, the recent efforts on the J-TEXT tokamak towards active control of the m/n = 2/1 tearing mode will be presented by applying the resonant magnetic perturbations (RMP).

In J-TEXT, two sets of saddle coils [8] have been constructed to control the TM. The static RMP coils, so called SRMP coils, are equipped outside the vacuum vessel and mainly produces static m/n = 2/1 and 3/1 RMP. The in-vessel RMP coils, which is named as DRMP, can generate either static or dynamic RMP with a maximum rotational frequency up to 6 kHz and dominant resonant modes of m/n = 2/1, 3/1 or 1/1. Previous experimental [9, 10] and theoretical [10, 11] studies showed that the RMP influences both the rotation and the width of the TM. As a result, the static RMP could apply a net stabilizing and braking effect on a rotating TM. The numerical modeling shows that a smaller amplitude of TM can be suppressed more easily by RMPs [9], suggesting that it is possible to take advantage of RMPs to control the precursor TM for disruption mitigation. With this motivation, the effect of RMP on high density limit and low-q limit discharges is studied on J-TEXT

tokamak [12]. It is found that a moderate amplitude of applied RMPs increases the density limit and delays the disruption, and the disruption precursor is suppressed with a slight reduction in toroidal plasma rotation.

However, the static RMP with significantly large amplitude could induce a large locked mode and the major disruption would follow it [13]. Thus, two strategies for controlling the TM have been proposed and tested in J-TEXT by applying the pulsed or fast rotating RMPs. To introduce those strategies, the rotating RMP is presented in section 2. In section 3, the method of identifying the phase of TM and warning of mode locking is described. The numerical simulation result of the pulsed RMP controlling the TM is carried out in section 4 and the confirmatory experiment is following. The investigations of fast rotating RMP are exhibition as follows: accelerating TM in section 5.1, unlocking the locked mode in section 5.2 and avoiding the locked mode induced disruption in section 5.3. The last section offers conclusions.

2. RMP SYSTEM ON J-TEXT TOKAMAK:

The distribution of DRMP is shown in Fig. 1. To generate the rotating RMP, two power supplies [14], with 90° phase difference between them, were used to feed ac currents with the waveform of $I_C = I \times \sin(2\pi f_{AC} t + \delta_i)$ into the DRMP coils. The f_{AC} is the frequency of the ac current within the range of 1 ~ 6 kHz, while the δi represents the phase of ac current in DRMP coil as listed and marked by the different colors in **Error! Reference source not found.**. The δ_i in each row of DRMP coils were selected to increase 90° successively with the toroidal direction. Hence, a RMP field with toroidal mode number n = 1 and rigidly rotating in the counter-Ip direction was generated at the frequency of $f_{RMP} = f_{AC}$. The δ_i in each column were

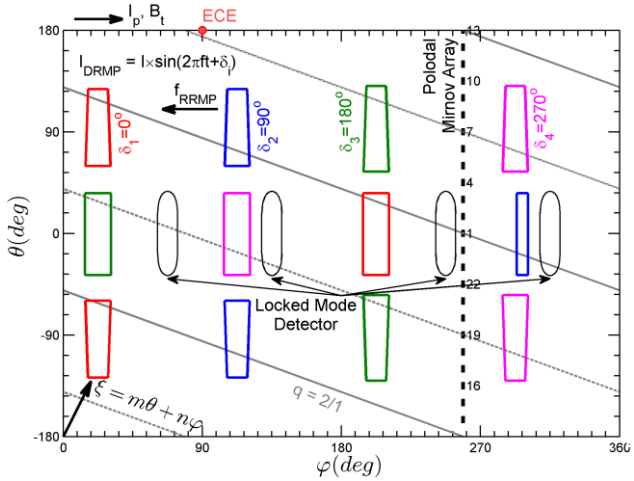

Fig. 1 The toroidal arrangement of the DRMP coils (thick lines), the poloidal Mirnov array, the locked mode detector and the ECE in J-TEXT tokamak. The field lines at the q = 2 resonant surface are also plotted with a straight field line assumption. The phases of ac currents in DRMP coils are marked for the top row and indicated by the colour for the rest. the red /blue coils connected with the green/magenta coils respectively, but the current direction is in opposi. A coordinate is defined by $\xi = m\theta + n\varphi$, where m = 2 and n = 1 is used.

selected to increase 180° successively from top to bottom to guarantee that the n = 1 RMP field had a dominate poloidal mode number of m = 2. Because the 2/1 tearing mode (TM) was only observed to rotate in the counter-Ip direction so far in J-TEXT, the counter-Ip direction is defined as the positive direction for both 2/1 tearing mode (TM) and the rotating RMP field. The rotating RMP rotating in co-Ip direction can be obtained by changing the phase difference between two AC power form 90° to -90°. The DRMP coils can induce eddy currents in the wall and the corresponding attenuation effect saturates above 1 kHz. The $\delta^{2/1}$ decreases with f_{AC} and the $b_r^{2/1} = 0.55$ Gauss/kA at the last closed surface (r = a) for the rotating RMP.

3. FAST ISLAND PHASE AND FREQUENCY IDENTIFICATION

It is very important to identify the helical phase, $\delta^{2/1}$, and the frequency f_{TM} of TM in real time for the TM control. When the O-point or X-point of the TM passes through the probe, the signal will experience a zero-crossing. A poloidal Mirnov probes array and a corresponding island phase identification method [15] are presented. We could measure helical phase $\delta^{2/1}$ (t) in real time by recording the time of each probes crossing zero. FIG. 2 demonstrates the process of tearing mode identification. We simulate a magnetic island, which mode number is 1 and is rotating at 1.5 kHz, shown in top diagram of left side of FIG. 2. Ten Mirnov probes are used to measure the island phase with the same color with the corresponding

signals at top diagram of right side FIG. 2. Multi-channel zero crossing comparison is used to deal with those Mirnov signals and pick out the points of time when the signal crosses zero. Each point could give the helical phase difference between TM and the 1st. Mirnov probe at this moment obtained by function (FIG. 2 middle diagram of right side). Then, the tearing mode phase could be measured in real time (FIG. 2 bottom diagram of right side). Also, the time difference means the average f he h ne [

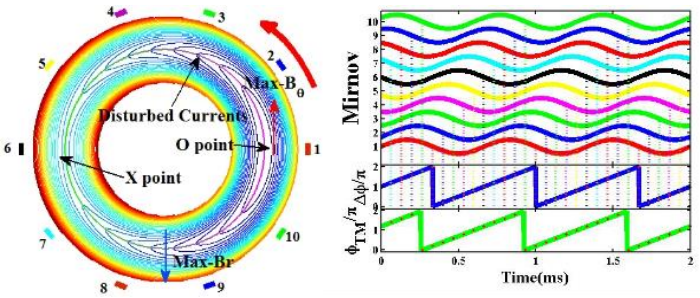

FIG. 2 (left figure) Island structure and probes position. (right figure) Ten simulated Mirnov signals in top diagram and phase difference between TM and 1st Mirnov probe (middle diagram) and phase of tearing mode measured in real time (bottom diagram).

4. THE PULSED RMP

It is clear from existing experimental and theoretical results that TM and plasma can be influenced by externally applied RMP [9, 17]. The effects of static RMP on the TM is depended by the phase difference Φ between them. when $0.5\pi < \Phi < 1.5\pi$ ($-0.5\pi < \Phi < 0.5\pi$) the effects is stabilizing (destabilizing) on the TM, when $\pi < \Phi < 2\pi$ ($0 < \Phi < \pi$) RMP contribute an accelerating (decelerating) effect on TM rotation[10]. While for the NTM, static RMP usually causes mode locking rather than

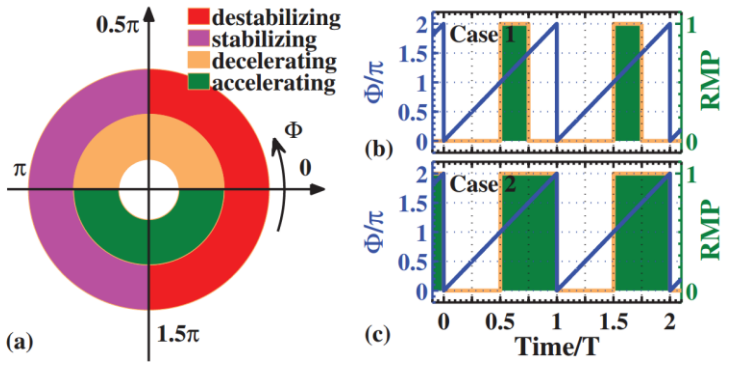

Fig. 3. (a) Diagram of the effects of RMP on TM. RMP is applied in phase region of (b) Case 1: $\pi < \Phi < 1.5\pi$, and (c) Case 2: $\pi < \Phi < 2\pi$. T is the island rotation period.

mode stabilization [17] The diagram of these effects is shown in figure 3(a). A new method is investigated for stabilizing the NTM as well as for accelerating the TM rotation: to apply static RMP only when $\pi \leqslant \Phi \leqslant 1.5\pi$ via feedback control of the RMP amplitude, as shown in Fig. 3 (b). During this region, the RMP only accelerate and stabilize the TM. Another method is applying the RMP during $\pi \leqslant \Phi \leqslant 2\pi$, as Fig 3 (c) showing, for the RMP could effect the TM with a longer time. The applied pulsed RMP will speed up the TM rotation more significantly, and the NTM is more stable with increased rotation [18], as observed on DIII-D [19]. On the other hand, the RMP will contribute a net stabilizing effect on NTM, since the island spends more time in the stabilizing region than in the destabilizing region due to rotation acceleration.

Nonlinear numerical modeling based on reduced MHD equations has been carried out by using the initial value code TM1[20]. It is found that the

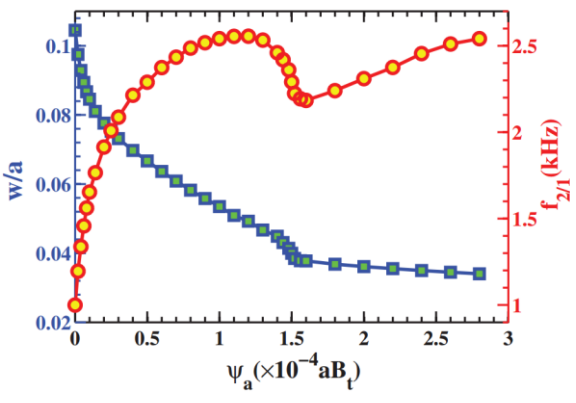

Fig. 4. Case 2: the saturated island width w/a (blue squares) and mode frequency $f_{2/1}$ (red circles) are shown as a function of RMP amplitude ψ_a.

NTM can be effectively suppressed, and the mode frequency is increased with this method.

For the Case 1, the time evolution of island width w/a and mode frequency $f_{2/1}$ are shown with $\psi_a = 5 \times 10^{-5}$, 2×10^{-4} and $3 \times 10^{-4} a B_t$ in the Fig. 3. The stronger RMP leads to the smaller island width, while the mode frequency first increases with the RMP amplitude and then decreases with it. The electromagnetic force exerted on the island by the RMP is proportional to ψ_a and the square of the island width, so that the change of the mode frequency is non-monotonic with time and increasing RMP amplitude. When the RMP is applied as the Case 2 method ($\pi < \Phi < 2\pi$), the results are shown in figure 4. It is found that the width of TM decrease with increasing RMP amplitude, and the mode rotation increase. However, for strong enough RMP with $\psi_a > 1.56 \times 10^{-4} a B_t$, the island width decreases slightly, while the mode frequency increases linearly with RMP amplitude. In this condition, it is found that the global plasma rotation is increased. The simulation results suggest that the strong enough pulsed RMP can suppress the NTM to a low level.

To confirm this new method of control the TM, a feedback control system and a pulsed RMP power supply are developed [21]. A poloidal Mirnov probes array serves the original signal to the feedback control system [16], which controller is field-programmable gate array (FPGA). By the method of introduced in section 2, the feedback system could identify the phase of TM in real time and create the pulse signal, which is used to control the pulse RMP power supply. The pulse power supply is open-loop controlled power, which work frequency could reach 6kHz and the maximum current is around 1kA. Fig. 5 is the diagram of the integral feedback pulse RMP system.

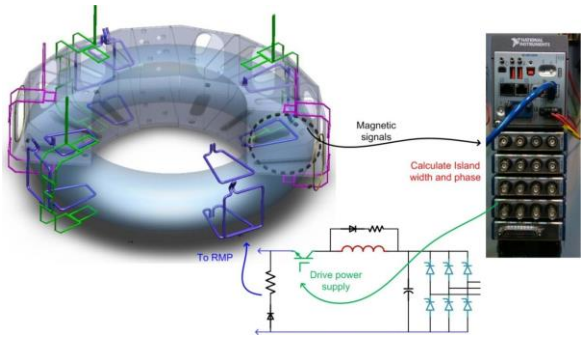

Fig. 5. The diagram of the feedback pulse RMP system, which is combined with FPGA, a poloidal Mirnov Probes array, DRMP coils and the pulse power supply.

For the large TM in the low q discharge, The pulse RMP's effects is insignificant, due to the finite amplitude of pulse RMP. When the pulse RMP works only within the region of $136^\circ < \Phi < 361^\circ$, the TM is accelerated and the mode frequency increasing about 10%. When the pulse RMP works only within the region of $278^\circ < \Phi < 98^\circ$, the TM's mode frequency decelerate about 10%. It's too difficult to identity the effects of pulse RMP on the width of TM. The statistic result of mode frequency difference with pulse RMP applied region is shown in Fig. 6. The $\Delta\xi$ means the start phase of applying pule RMP, which is under the assumption of the RMP works only half of mode rotation cycle. Base on the theory of the effects of RMP on TM, the mode frequency difference should have a cosine relationship with the pulse RMP applied region. The phase shift is caused by the eddy current induced the measurement error. The effective of the new control method is confirmed in experiment.

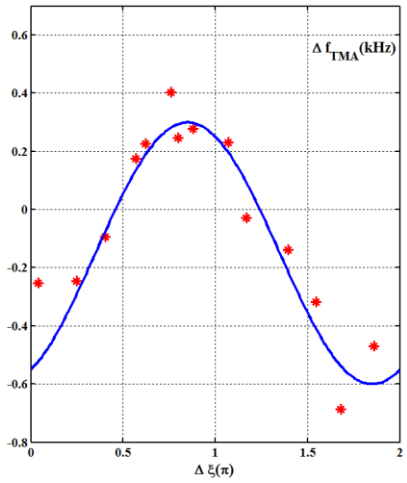

Fig. 6. The statistic result of mode frequency difference with pulse RMP applied region. Red points are experience results, the blue line is fitting line of the experiment.

5. FAST ROTATING RMP

5.1 Accelerating the TM

Comparing with the static RMP, a rotating RMP is more controllable in terms of frequency and phase of the external field. An existing TM is very likely to be locked to the rotating RMP and then rotates synchronously with the external field [22]. The plasma current and the toroidal field are set as 200 kA and 1.8 T, respectively. The DRMP operates at 5 kHz and the frequency remains unchanged throughout the discharge as shown in Fig. 7. After the rotating RMP is switched on at 0.25 s, the mode frequency, which is calculated by performing time-frequency analysis on dBθ/dt, starts to increase. When the current of rotating RMP reaches a threshold, approximately 0.6 kA in this shot, the mode frequency jumps abruptly from 4.5 kHz to 5 kHz, which is the frequency of the rotation RMP. Then the mode frequency remains at 5 kHz until the rotating RMP current drops to a small level, at which point the island is unlocked from the rotating RMP. Meanwhile, the edge plasma rotation measured by the Doppler shift of the spectrum of C-V radiation, changes toward the counter-current direction. Further investigation [22] suggest that the electromagnetic torque of RMP have a more obvious the effect on the TM when the frequency difference between TM and rotating RMP is smaller.

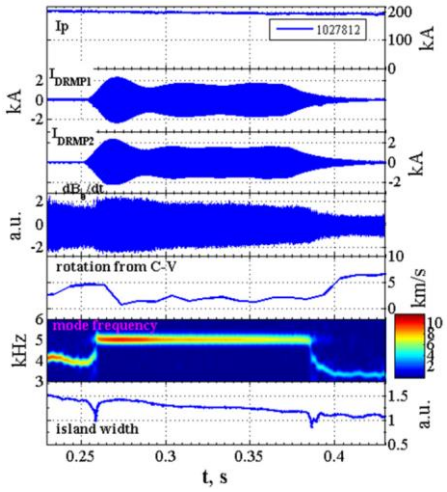

Fig. 7. Signals including plasma current, current of DRMP, dBθ /dt , edge plasma rotation, mode frequency and island width in a typical mode locking process to DRMP. The magnetic island is locked to DRMP at 0.26 s and unlocked at 0.385 s. The color in the frequency panel stands for the strength of a certain frequency component of the Mirnov signal.

5.2 Rotating RMP unlock the locked mode

After achieving the acceleration of TM by the higher frequency rotating RMP, a straightforward idea is driving the locked mode by exert additional electromagnetic torque generated by the rotating RMP [23]. To study the unlocking of LM and the corresponding process, static RMP (Fig. 8 (a)) was used to lock the TM and maintain a static 2/1 LM for approximately 200 ms. The amplitude of static RMP was limited for the non-disruption discharging. After mode locking, the rotating RMP (Fig. 8 (b)) was applied to drive the locked mode from the static state and unlocked it. The contour plot of Mirnov integral signals (Fig. 8 (g)) indicating that the unlocking process exhibits two stages, i.e. the oscillating stage and the unlocking stage. The oscillating stage (t < 0.32 s) is similar to that shown in Fig. 8 (f), because the amplitude of rotating RMP is not strong enough. When the mode phase decreases more than 0.5π, the locked mode was unlocked by the rotating RMP and the TM was rotating with rotating RMP synchronously.

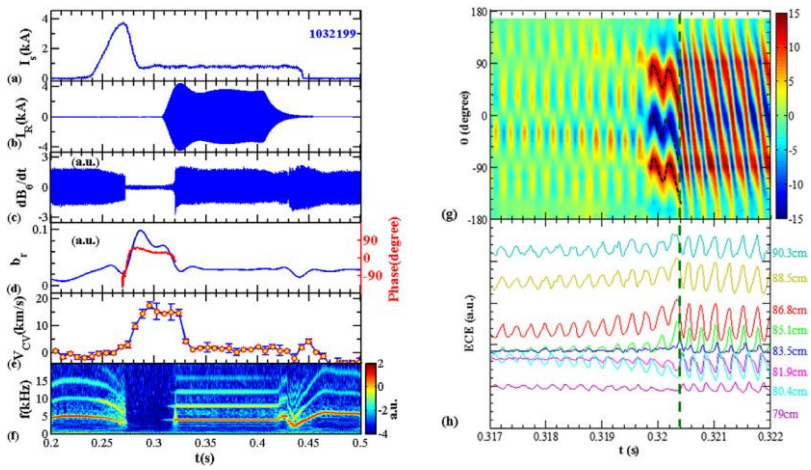

Fig. 8. Time evolution of LM unlocking for shot 1032199 : (a) static RMP coil current Is , (b) rotating RMP coil current IRwith a frequency is 4 kHz, (c) Mirnov signal dBθ/dt, (d) LM detector signal br (blue curve) and the phase of magnetic island during mode locking (red curve), (e) plasma toroidal rotation VCV, (f) 2/1 TM frequency f , (g) the contour plot of Mirnov integral signals in the interval of 0.317 s < t < 0.322 s, and (h) time evolution of ECE signals.

5.3 Avoiding the locked mode induced disruption

Many disruption is induced by locked mode, especially the 2/1 tearing mode. Whither avoiding or unlocking the locked mode could avoid the disruption? With this purpose, the rotating RMP is applied before the mode locking by feedback. The rotating RMP could force the TM rotating with its frequency and suppress the tearing mode slightly. The experiment results is the disruption would be avoided or delayed after the mode locking be avoid in the experiment.

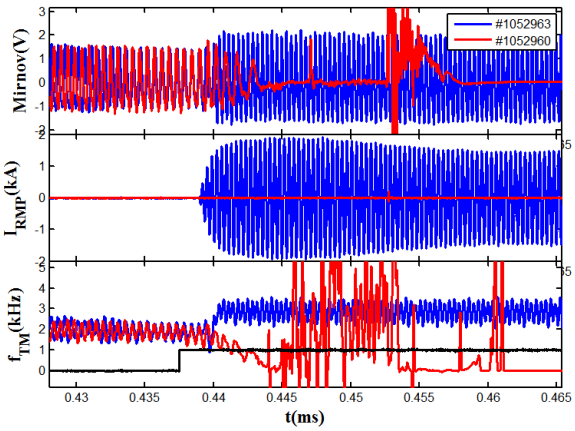

Fig. 9. The locked mode induced disruption and avoiding the disruption via the rotating RMP. The time evolution of Mirnov signals (upper figure), the current of rotating RMP (middle figure) and the frequency of the TM (bottom figure). The classical shot of locked mode induced disruption (red lines) is compared with the shot of disruption avoidance (blue lines). The black line in bottom figure is the trigger signal.

When the edge safe factor q_a close the low-q limit, the disruption is triggered by the mode locking and the discharges are repeatable. A classical shot about the locked mode induced disruption is shown in Fig. 9 (red lines). With the increasing plasma current, the amplitude of tearing mode was stable and increasing after the current is higher than a certain threshold. When the amplitude of the tearing mode is larger than a certain threshold, the rotating frequency of tearing mode would drop to zero and the disruption would occur few or tens of milliseconds latter. The rotating RMP (blue lines in Fig. 9) is triggered by mode locking warning system (black line in the bottom figure of Fig. 9), which could measure the rotating frequency of tearing mode in real time and explore higher voltage when the tearing mode rotating slower than a certain threshold. Rotating RMP could accelerate and suppress the tearing mode before the tearing mode be locked. Comparing with the shot without applying rotating RMP, the mode locking and disruption are avoided after applying rotating RMP.

The statistical results is shown in the Fig. 10. Δt is the time difference between the mode locking warning and the disruption. The shots during which the 3kHz rotating RMP was applied are the blue points. When the amplitude of RMP is too small to accelerate the tearing mode, there, of course, has no effects on avoiding the disruption. If the rotating RMP could accelerate and lock the tearing mode, the disruption would be avoided, especially the points in the red dashes oval. However, with the increasing of rotating RMP amplitude, the Δt is shorter and shorter. This phenomenon is caused by the enhancement of RMP on the tearing mode. Another group of shots shows the different effects of different rotating frequency of RMP. The shot of applying 3kHz rotating RMP has a very significant improvement comparing with the lower frequency case, as the purple arrow shows in Fig. 10. The cases of applying 2kHz and 1kHz rotating RMP seems to have bad effects on avoiding disruption comparing the shots without rotating RMP. But, if the rotating RMP is applied just before the frequency of tearing mode dropping to zero, the mode

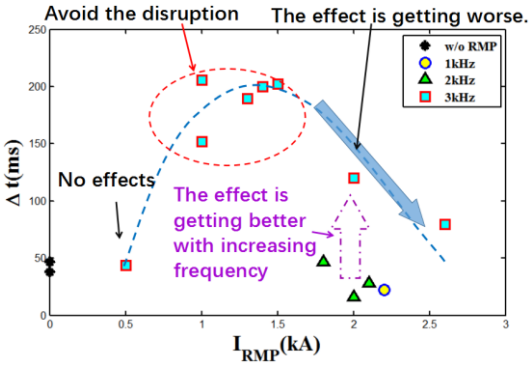

Fig. 10 The statistic result of rotating RMPs with different frequencies and amplitudes effect the disruption. Δt is the time difference between the mode locking warning and the disruption. The black point, yellow circle, green triangle and green square are the results of no RMP and applying rotating RMP with 1kHz, 2kHz and 3 kHz, respectively.

locking would be avoid so as to the disruption. So the statistical analysis suggest two important conclusions: the rotating RMP with higher frequency has a better effects and the amplitude of rotating RMP should be limited to get the best effect.

6. CONCLUSION

MHD instability control has been investigated for a long term on the J-TEXT tokamak. The effects of RMP on the TM has been studied in both experiment and numerical simulation. Base on the previous results, two strategies for controlling the TM have been proposed and tested in J-TEXT by applying the pulsed or fast rotating RMPs.

The first control strategy is to apply pulsed RMP to the TM only during the accelerating phase region. With the nonlinear simulation code TM1, the pulsed RMP is proved to have the ability of accelerating the mode rotation TM and even completely suppressing the mode. Besides, it is found that the frequency of TM is non-monotonic with the increasing amplitude of the pulsed RMP. The followed experimental attempt with the pulsed RMP at relative low amplitude has demonstrated the acceleration effect, so as to the relationship between the dynamic results and the phase region of applying the pulsed RMP, which accord with the theoretical expect.

The second control method is applying the fast rotating RMP field before mode locking, which has been successful for the avoidance of mode locking and the prevention of plasma disruption. The rotating RMP was triggered by mode locking warning system in the discharges of closing low-q limit and accelerated the mode. As a result, the disruption was prevented. In experiment, the 3 kHz rotating RMP has the best performance comparing the rotating RMP with lower frequency. However, the benefit of rotating RMP on the disruption control was not monotonous with its amplitude.

ACKNOWLEDGMENT

The authors would like to thank the members of the J-TEXT team for their assistance in the experiment. This work is supported by National Magnetic Confinement Fusion Science Program of China (Contract No. 2014GB118000, 2015GB111001 and 2013GB106003B) and the National Natural Science Foundation of China (Contract No. 11275080, 11405068 and 11505069). N.W. is thankful for the support from the China Scholarship Council.

REFERENCE

[1] H. P. Furth Physics of Fluids **16**, (1973).

[2] P. H. Rutherford Physics of Fluids **16**, (1973).

[3] R. J. La Haye, R. Fitzpatrick, T. C. Hender, A. W. Morris, J. T. Scoville and T. N. Todd Physics of Fluids B: Plasma Physics **4**, (1992).

[4] R. B. White, D. A. Monticello and M. N. Rosenbluth Physical review letters **39**, (1977).

[5] T. Casper, Y. Gribov, A. Kavin, V. Lukash, R. Khayrutdinov, H. Fujieda and C. Kessel Nuclear Fusion **54**, (2014).

[6] M. Shimada, D. J. Campbell, V. Mukhovatov, M. Fujiwara, N. Kirneva, K. Lackner, M. Nagami, V. D. Pustovitov, N. Uckan, J. Wesley, N. Asakura, A. E. Costley, A. J. H. Donné, E. J. Doyle, A. Fasoli, C. Gormezano, Y. Gribov, O. Gruber, T. C. Hender, W. Houlberg, S. Ide, Y. Kamada, A. Leonard, B. Lipschultz, A. Loarte, K. Miyamoto, V. Mukhovatov, T. H. Osborne, A. Polevoi and A. C. C. Sips Nuclear Fusion **47**, (2007).

[7] Y. Wan, J. Li, Y. Liu, X. Wang, V. Chan, C. Chen, X. Duan, P. Fu, X. Gao, K. Feng, S. Liu, Y. Song, P. Weng, B. Wan, F. Wan, H. Wang, S. Wu, M. Ye, Q. Yang, G. Zheng, G. Zhuang and Q. Li Nuclear Fusion **57**, (2017).

[8] B. Rao, G. Wang, Y. H. Ding, K. X. Yu, Q. L. Li, N. C. Wang, B. Yi, J. Y. Nan, Y. S. Cen, Q. M. Hu, W. Jin, J. C. Li, H. Jin, M. Zhang and G. Zhuang Fusion Engineering and Design **89**, (2014).

[9] Q. Hu, Q. Yu, B. Rao, Y. Ding, X. Hu and G. Zhuang Nuclear Fusion **52**, (2012).

[10] Q. Hu, B. Rao, Q. Yu, Y. Ding, G. Zhuang, W. Jin and X. Hu Physics of Plasmas **20**, (2013).

[11] R. Fitzpatrick Physics of Plasmas **2**, (1995).

[12] Q. Hu, N. Wang, Q. Yu, Y. Ding, B. Rao, Z. Chen and H. Jin Plasma Physics and Controlled Fusion **58**, (2016).

[13] Y. Ding, X. Jin, Z. Chen and G. Zhuang Plasma Science and Technology **15**, (2013).

[14] B. Yi, Y. H. Ding, M. Zhang, B. Rao, J. Y. Nan, W. B. Zeng, M. Y. Zheng, H. Y. Xu, G. Zhuang and Y. Pan Fusion Engineering and Design **88**, (2013).

[15] B. Rao, D. Li, F. R. Hu, Y. H. Ding, Q. M. Hu and H. Jin The Review of scientific instruments **87**, (2016).

[16] W. Zheng, F. Hu, M. Zhang, D. Li, Q. Hu, H. Jin, B. Rao, M. Yan, Y. Pan and K. Yu IEEE Transactions on Nuclear Science **65**, (2018).

[17] S. Fietz, A. Bergmann, I. Classen, M. Maraschek, M. Garcia-Muñoz, W. Suttrop and H. Zohm Nuclear Fusion **55**, (2015).

[18] Q. Hu, Q. Yu and X. Hu Physics of Plasmas **21**, (2014).

[19] R. J. La Haye, C. C. Petty and P. A. Politzer Nuclear Fusion **51**, (2011).

[20] Q. Yu, S. Günter and K. Lackner Physics of Plasmas **11**, (2004).

[21] M. X. Yan, B. Rao, Y. H. Ding, Q. M. Hu, F. R. Hu, D. Li, M. Li, X. K. Ji, G. Xu, W. Zheng and Z. H. Jiang Fusion Engineering and Design **115**, (2017).

[22] B. Rao, Y. H. Ding, Q. M. Hu, N. C. Wang, B. Yi, M. Y. Zheng, W. Jin, J. C. Li, Z. F. Cheng, Q. Yu, K. X. Yu and G. Zhuang Plasma Physics and Controlled Fusion **55**, (2013).

[23] H. Jin, Q. Hu, N. Wang, B. Rao, Y. Ding, D. Li, M. Li and S. Xie Plasma Physics and Controlled Fusion **57**, (2015).